اونيۇرسيتى مليسيا ڤهڠ
UNIVERSITI MALAYSIA PAHANG

ORIGINAL ARTICLE

Transient Elastohydrodynamic Lubrication of Rough Contact Surface for Intermittent Motion

M.F. Abd Al-Samieh

Mechanical Design & Production Department, Military Technical College, El-qobba Bridge Cairo, Egypt

ABSTRACT – The current study aims to study the characteristics of transient elastohydrodynamic lubrication of smooth and rough surface contacts subjected to intermittent motion for different inactive periods of motion and deceleration/acceleration periods to fulfill an identified need for such conjunction. In this case, the non-steady Reynolds' equation, the film thickness equation with elastic deformation and taking into account the influence of surface roughness, and the load balance equation are simultaneously solved using the Newton-Raphson with Gauss-Seidel iterations method to determine the film profile and pressure distribution at various time steps. Surface contact of sinusoidal waves is presented with different amplitudes and wavelengths. The results indicated that surface waviness causes random oscillations in pressure and film profiles at different time steps. The greater the amplitude of the waviness, the more pressure and film profile variations occur. The magnitude of the pressure and film profile fluctuations becomes little noticeable as the wavelength of a wavy surface rises. The findings of this investigation also revealed that increasing the inactive duration for wavy surfaces results in zero minimum film thickness and surface contact. Squeezing action is ineffective in conveying loading capacity in this circumstance. The central and maximum pressure heights increase during the stop time interval as stop time increases. The centre film thickness increases at the end of the deceleration phase when the deceleration/acceleration period is reduced, but the minimum film thickness is unaffected. In fact, the minimum film thickness tends to be zero at the end of the deceleration phase, regardless of the deceleration/acceleration period. The central and maximum pressure increase during the stop time interval with the decrease of the deceleration/acceleration period. The difference between the results for smooth and wavy surface contacts is the appearance of fluctuations in film and pressure profiles, as well as the reduction of the film thickness and increase in pressure for the wavy surface when compared to contact with a smooth surface.

NOMENCLATURE

A	Dimensionless amplitude	P_{Her}	Hertzian contact pressure
b	Hertzian contact radius	η	Viscosity of lubricant
h	Lubricant film thickness	α	Viscosity pressure coefficient
H	Film thickness in dimensionless form, $H=hR/b^2$	η_0	Atmospheric lubricant viscosity
H_0	Central film thickness in dimensionless form	ρ	Density of lubricant
l	Lateral leakage limit distance	ρ_o	Atmospheric density of lubricant
m	Entrance distance	λ	Dimensionless wavelength
p	Hydrodynamic pressure	t_d	Deceleration/acceleration period
P	Hydrodynamic pressure in dimensionless form, $P=p/P_{Her}$	t_s	Stop period

INTRODUCTION

The effect of roughness was important in elastohydrodynamic lubrication, especially when the surface roughness was comparable to the film thickness. Mechanical components can be exposed to transient conditions that can damage the lubricant film, resulting in shorter service life of the component. In practical applications, lubricated contact surfaces are subjected to variations in the speed of the surfaces contact. For example, the operating cycle of cams, gears, and stepper motors exposed the bearings to rapid speed changes in a repeat sequence at the start-stop, resulting in squeeze film action, which led to a significant amount of pressure being generated between the contacts during the squeeze process, and as a result, an elastic dimple appears in the contacting surfaces. In order to extend the service life of tribological components and decrease wear and friction, it is important to understand the effect of contact surface waviness on transient elastohydrodynamic lubrication by squeeze action.

Several researches have been done to study the mechanisms of transient elastohydrodynamic lubricated contact for surface speed variations, for example, presented by Glovnea and Spikes [1, 2], Al-Samieh and Rahnejat [3], Petr et al.

[4], Ming et al. [5], Ohno [6], Sperka [7], Alsamieh [8], Meziane et al. [9, 10], and Sivayogan et al. [11]. All previous studies, both theoretically and experimentally, have shown that the thickness of the film observed during the transient action is contrary to the predicted values using the theory of steady-state elastohydrodynamics at instantaneous speed since the thickness of the film will be zero as the speed of entraining motion reaches a zero value, which contradicts the results of both experimental and numerical transient action. The results showed that a dimple film shape was formed for the portion of the cycle with the increasing squeeze effect.

Glovnea and Spikes [1, 2] experimentally investigated transient elastohydrodynamic for the fast halting, using an ultrathin interferometer to measure the lubricant film thickness and theoretically used the numerical solution of Grubin's for elastohydrodynamic lubrication. Their investigations showed that the centre film thickness at the last moment of the inactive phase has little dependence on the primary speed but very strongly on the deceleration rate. Immediately before the stoppage is complete, the film thickness at the inlet rapidly decreases to constitute an entrapment.

Recently, Duohuan et al. [12] theoretically studied the influence of variations of the squeeze elastohydrodynamic lubrication oil film in unidirectional and bidirectional intermittent motions for smooth contact surfaces. They studied the effects of varying stop time, acceleration/deceleration time, applied load, as well as the elliptic ratio in one-way intermittent motion on the characteristics of elastohydrodynamic lubricated smooth contact. Their investigations revealed that the change in the central and maximum pressures and central and minimum film thicknesses during the intermittent motion is the same as that of an impact-rebound process. The shape of the pressure versus time curve is also affected by the elliptic ratio and the applied load. They showed that for long intermittent period, the contact is actually a steady-state contact, so the characteristics of the oil film will be different from those of the oil film with a smaller intermittent period. Their results also revealed that for the same uniform entraining velocities, a decrease in acceleration time leads to a reduction in pressure and film thickness compared with a larger acceleration time and an increase in pressure and film thickness during stop time.

Surface roughness can be integrated with mathematical models that assume actual or artificial surface feature. While the actual feature is complicated to deal with it numerically, artificial feature processing is easier and common. Previously, the rough surfaces of elastohydrodynamic lubrication have been studied with two approaches. The first approach is the stochastic method, which has been pointed out by many researchers, such as Epstein et al. [13], Wang et al. [14], and Masjedi and Khonsari [15]. Another approach is the deterministic method (see for example, Jacod et al. [16], Yang et al. [17], LiMing et al. [18], Punit and Niraj [19], Linlin and Jiajun [20], Yang et al. [21], Alsamieh [22], Zhang [23], Hansena et al. [24], and Hultqvist et al. [25, 26, 27]). The results of all previous studies showed that the effect of surface roughness could not be ignored when studying oil film thickness and pressure in precision equipment. The pressure and film thickness profile will vary depending on the wavelength and amplitude. The existence of surface roughness results in unpredictable variations in pressure and film thickness, which can be more severe on rough surfaces.

To date, investigations of the characteristics of transient lubricated elastohydrodynamic rough contact surfaces exposed to intermittent motion have not been completed. Therefore, in this paper, the transient Reynolds equation, the film thickness equation incorporating the effects of elastic deformation and surface roughness, and the load equilibrium equation are to be solved using the Newton-Rapson with Gauss-Seidel iteration method. The effects of amplitude and wavelength changes on film and pressure profiles are visualized and analyzed at various time steps. The effects of varying the periods of the inactive motion and deceleration/acceleration on the characteristics of elastohydrodynamic lubricated smooth and rough contact surfaces are discussed and presented by the central and minimum film thicknesses and the central and maximum pressures throughout the contact zone.

BACKGROUND THEORY

The non-steady Reynolds equation can be presented dimensionless as follows:

$$\frac{\partial}{\partial X}\left(\frac{\bar{\rho}H^3}{\bar{\eta}}\frac{\partial P}{\partial X}\right) + \frac{\partial}{\partial Y}\left(\frac{\bar{\rho}H^3}{\bar{\eta}}\frac{\partial P}{\partial Y}\right) = \emptyset\left\{\frac{\partial(\bar{\rho}H)}{\partial X} + \frac{bE'}{\eta_0 u}\left(\bar{\rho}\frac{\partial H}{\partial \bar{t}} + H\frac{\partial \bar{\rho}}{\partial \bar{t}}\right)\right\}$$

(1)

where:

$$X = x/b, \ Y = y/b, \bar{\eta} = \eta/\eta_o, \ \bar{\rho} = \frac{\rho}{\rho_o}, H = hR/b^2, \ P = p/P_{Her}, \ \emptyset = \frac{12R^2\eta_0 u}{b^3 P_{Her}},$$

The density change due to pressure was given as shown below by Dowson and Higginson in 1959:

$$\bar{\rho} = 1 + \frac{\varepsilon P P_{Her}}{1 + \zeta P P_{Her}}$$

(2)

where, ζ and ε are constants depending on the lubricant type. The relationship between viscosity and pressure was proposed by Roelands in 1966 as follows:

$$\overline{\eta} = exp[ln\eta_o + 9.67][(1 + 5.1 * 10^{-9}PP_{Her})^Z - 1] \qquad , \qquad Z = \frac{\alpha}{5.1*10^{-9}[\ln\eta_\circ + 9.67]} \qquad (3)$$

Figure 1 shows the computational representation of the domain of the elastohydrodynamic lubricated contact problem, where m and n are the entrance and exit lengths, respectively, and l is the lateral limit distance.
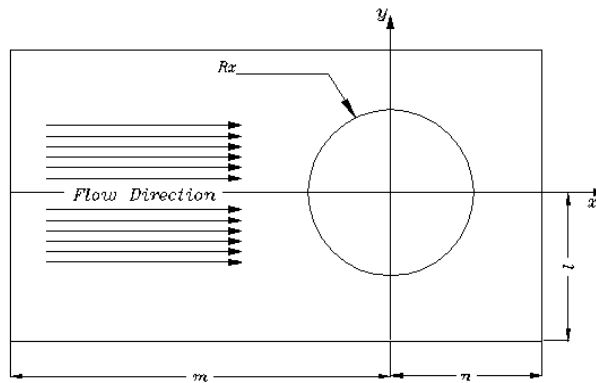
Figure 1. Computational representation of the domain.

The equation for the film thickness can be given as (see Gohar and Rahnejat [28] and AlSamieh [29]):

$$H(X,Y,T) = H_0(T) + \frac{(X-m)^2}{2} + \frac{(Y-l)^2}{2} + \frac{R\delta(X.Y.T)}{b^2} + Asin\left(\frac{2\pi X}{\lambda}\right)sin\left(\frac{2\pi Y}{\lambda}\right) \qquad (4)$$

The third term in Eq. (4) represents the elastic deformation and can be represented by:

$$\delta_{I,J}(x,y) = \frac{2}{\Pi}\sum_{j=1}^{ny}\sum_{i=1}^{nx}P_{i,j}D_{i^\circ j^\circ} \qquad (5)$$

where, $i^\circ = |I-i|+1, j^\circ = |J-j|+1$. The last term of the film thickness Eq. (4) represents the hypothetical sinusoidal surface topography where A and λ are the amplitude and wavelength in dimensionless, respectively. The Newton-Raphson method is applied to solve the Reynolds' equation in the following form (see AlSamieh [22]):

$$\sum_{l=2}^{N}\sum_{k=2}^{M}\frac{\partial F_{i,j}(t)}{\partial P_{k,l}}\Delta P_{k,l} = -F_{i,j}(t) \qquad (6)$$

The above Eq. (6) can be rewritten using the Gauss-Seidel iteration technique as follows:

$$\Delta P_{k,l}^n = \frac{(-F_{i,j} - J_{k-1,l}^{i,j}\Delta P_{k-1,l}^n - J_{k+1,l}^{i,j}\Delta P_{k+1,l}^{n-1} - J_{k,l-1}^{i,j}\Delta P_{k,l-1}^n - J_{k,l+1}^{i,j}\Delta P_{k,l+1}^{n+1})}{J_{k,l}^{i,j}}, where\ J_{k,l}^{i,j} = \frac{\partial F_{i,j}(t)}{\partial P_{k,l}} \qquad (7)$$

Using under-relaxation factor, the pressure can be evaluated in accordance to:

$$P_{i,j}^n = P_{i,j}^{n-1} + \Omega\Delta P_{i,j}^n \qquad (8)$$

In Eq. (8), Ω is the relaxation deficiency factor, its value in the range (0.01-0.02). The pressure convergence criterion is:

$$\left[\frac{\sum_{j=1,2,..}^{U}\sum_{i=1,2,..}^{V}\left(P_{i,j}^n - P_{i,j}^{n-1}\right)^2}{UxV}\right]^{0.5} \leq 10^{-3} \qquad (9)$$

The convergence criterion for load balancing is:

$$\left| \iint P(X,Y)dXdY - \frac{2}{3}\pi \right| \le 10^{-4} \tag{10}$$

where, U and V are the whole grid points in X and Y directions.

RESULTS AND DISCUSSION

Table 1 lists the lubricants, materials, and working parameters used in the present study. All the cases presented in this paper use an extended domain in the X-direction from - 2.5 to 2.5 and in the Y-direction from -1.6 to 1.6 to guarantee completely flooded conditions and fulfill the convergence criterion using a net grid point of 75×70 in the rolling and transverse directions, respectively. The time step selected in this analysis is Δt = 0.04ms. In fact, the selection of the total mesh size in both directions of rolling and transverse and the time increase is based on the fact that, by further increasing the node density in both rolling direction and transverse direction and the time step, the corresponding result film and pressure profiles can not be affected, and it can achieve rapid convergence of the solution at each time step. In the current analysis, the solution has to be reached within (2500–3500) steps during non-steady action. The total task processing time on a 3 GHz i5 CPU computer is roughly (8-12) hours. The entraining velocity versus time graph of the intermittent motion shown in Figure 2 was used by Duohuan et al. [12] and is applied to all conditions described in this paper. Duohuan et al. [12] assumed that a contact applied normal load of 75 N is used at a controlled lubricant temperature of 20ºC.

Table 1. Lubricant, material, and working parameters.

Designation	Names	Values
η_o	Viscosity	1.38 Pa.s
α	Viscosity coefficient for pressure	28 GPa^{-1}
ε	Used constant in Eq. (2)	5.83x10^{-10} Pa
ξ	Used constant in Eq. (2)	1.68x10^{-9} Pa
E'	Equivalent modulus of elasticity	226 GPa
R	Equivalent radius of curvature	0.0127 (m)
w	Load	75 N
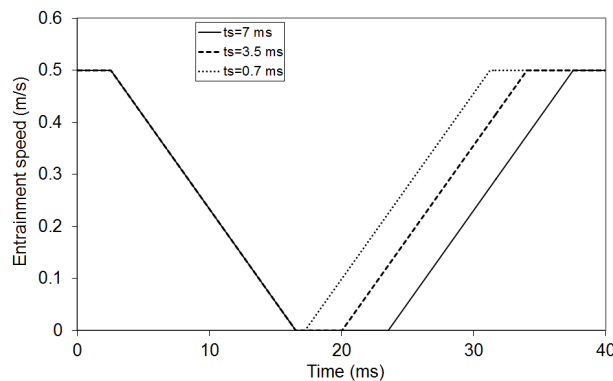
Figure 2. Speed variation with time.

Comparison between the results of the current numerical solutions and those developed by Duohuan et al. [12] for smooth surfaces contact at the operating conditions shown in Table 1 are presented in detail in Figure 3 and 4 for a deceleration/acceleration period of 14 ms and an inactive period of 7 ms. These figures show the film profile and pressure distribution at various time steps in the direction of entraining motion through the central film; that is shown in Figure 3 presented by Duohuan et al. [12], and that is shown in Figure 4 for the current numerical result. It is clear that the present numerical solution conforms well with those presented by Duohuan et al. [12].

Film profile and pressure distribution at t = 1.75 sec (see Figure 3(a) and 4(a)) are the results at a maximum speed of 0.5 m/s before the motion starts to decelerate. In this period, wedge action is dominant and the squeeze action effect is neglected. At the last instant of the deceleration period at t=15.75 ms, the pressure spike increases rapidly as the lubricant is entrapped between the two mating surfaces; see Figure 3(b) and 4(b). In this period, the effect of wedge action reduced and the action of squeeze effects became responsible for film thickness formation. At the last instant of inactive period at t=22.75 ms, the entrapped oil flows outside of the contact area leads to increase in the pressure at the periphery region, which appears as two pressure spikes, see Figure 3(c) and 4(c). As the motion has been restarted, the wedge action again increases with the increase of the entraining motion; see Figure 3(d), 3(e) and 4(d) to 4(g) at different snapshots of time (of 24.5, 25.5, 26.5 and 27.12 ms), respectively. During this period, the entrapped oil is removed outside of the contact so that the film profile resembles a wedge shape with a small pressure spike; see Figure 3(e) and 4(g). Finally, at t = 36.75 ms (the contact speed reaches its maximum value), the effect of wedge action takes over, as shown in Figure 3(f) and 4(h), and the film thickness and pressure profile shape resemble those shown in Figure 3(a) and 4(a) at the start of entraining motion.

(a) t = 1.75 ms   (b) t = 15.75 ms   (c) t = 22.75 ms

(d) t = 24.5 ms   (e) t = 27.125 ms   (a) t = 36.75 ms
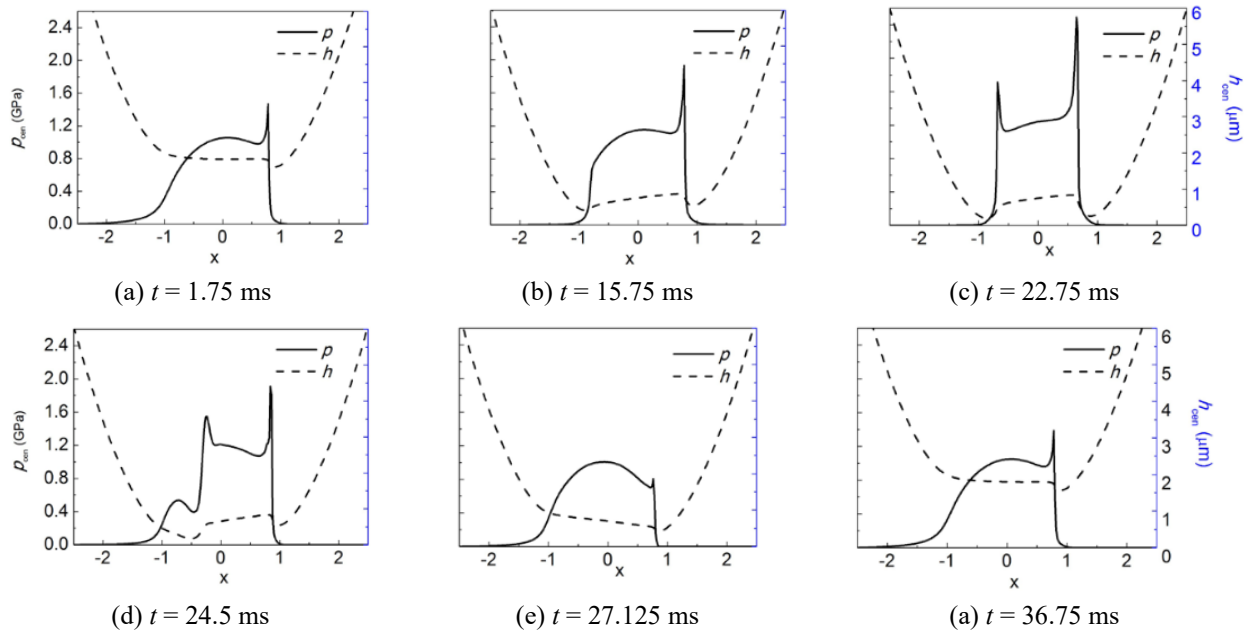
Figure 3. Film profile and pressure distribution in the contact center after Duohuan et al. [12].

(a)

(b)

(c)

(d)

(e)

(f)
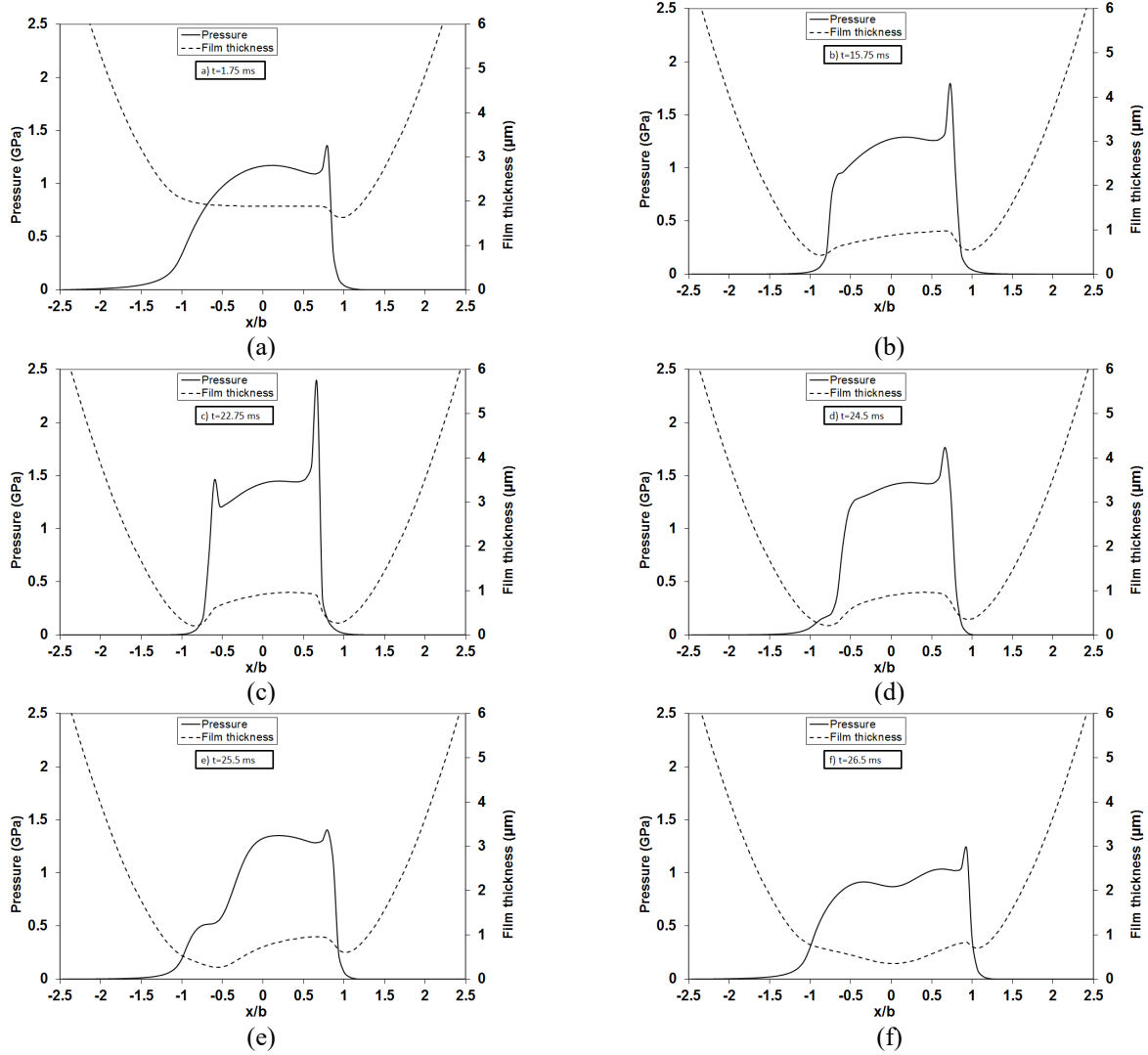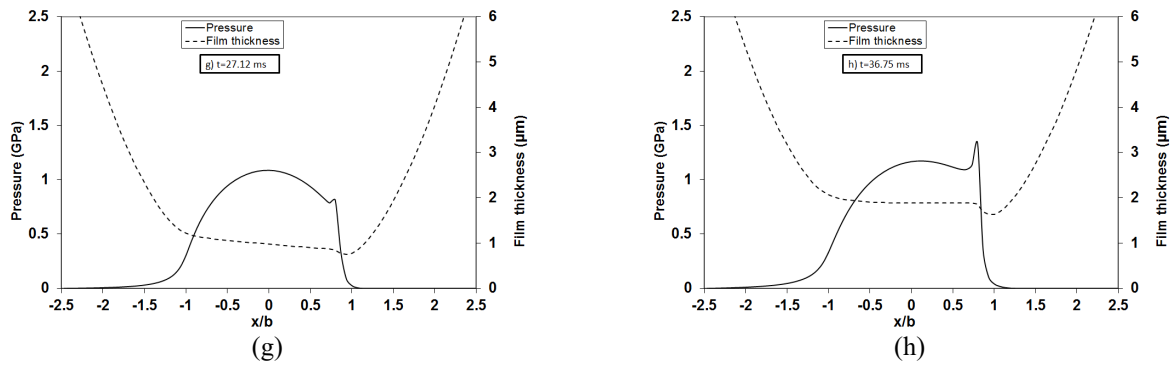
Figure 4. Numerically predicted film profile and pressure distribution in the contact center.

Figure 5 shows the characteristics of the lubricated conjunction presented by central and maximum pressure and central and minimum film thickness for various inactive periods of 7, 3.5, and 0.7 ms at a deceleration/acceleration period of 14 ms. At the uniform entraining speed of 0.5 m/s, the values of the central pressure, maximum pressure, central film thickness and minimum film thickness are 1.15 GPa, 1.6 GPa, 1.84 µm and 1.35 µm, respectively, while those obtained by Duohuan et al. [12] are 1.052 GPa, 1.65 GPa, 1.85 µm and 1.4 µm, respectively. The error is less than 8%. It is obvious that the central pressure settles at the uniform entraining speed at a value of 1.15 GPa, followed by a slow increase during the deceleration period, followed by a rapid increase during the stop time, followed by a rapid decrease. Then, the central pressure gradually increased to a value of 1.15 GPa, corresponding to the uniform speed of 0.5 m/sec. Center pressure height increases as stop time increases.
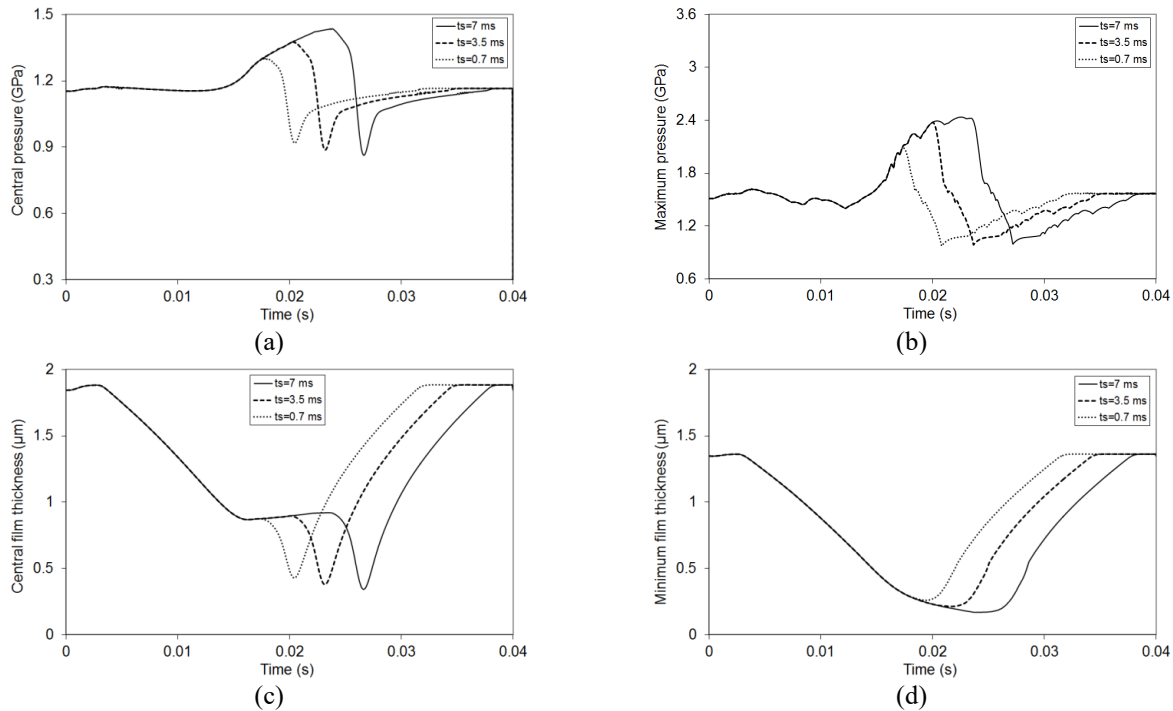
Figure 5. Characteristic of the lubricated smooth conjunction for different inactive periods.

It is seen that the maximum pressure is zigzag because of its position change over the contact area. Its value increases to more than 2.5 GPa during stop time and also increases with increasing stop time. At maximum entraining speed, the central film thickness is nearly equal to 1.82 m and decreases linearly with decreasing entraining speed. During the inactive period, the central film thickness is horizontal at about 0.85µm, followed by a constriction, which is the lowest film thickness—the lowest value of the central film thickness increases as the stop interval increases. Once the lowest part of the film thickness moves out of the conjunction, the central film thickness starts to increase again until it reaches 1.82 µm at the uniform entraining speed. The minimum film thickness decreases slowly during stop time, as one would expect from pure squeeze film action, and decreases with increasing stop time. The physical explanations for this feature are that the increased inactive period allows more trapped lubricant to flow out of the contact area, resulting in reduced central and minimal film thickness.

To see squeeze-action effect on film thickness formation within the period of intermittent motion, the squeeze-velocity ratio versus time is seen in Figure 6 for a 75 N applied load and entrainment speed pattern that is shown in Figure 2 for a maximum speed of 0.5 m/s for a deceleration/acceleration period of 14 ms and an inactive period of 7 ms. It is obvious that, initially, the entraining speed is maximum and that the wedge effect prevails in generating the load capacity as squeeze-velocity ratio of positive value occurs. This positive value does not affect the loading carrying capacity of the

contact surface. As a result of that, the film thickness of flat shape appears, and no indentation in the contact area confirms that the film thickness formation is due to the entraining speed; see Figure 3(a) and 4(a). During the deceleration period, the wedge action and squeeze action can be taken into account to determine the loading carrying capacity of the conjunction as a negative value of the squeeze effect occurs, resulting in dimple formation; see Figure 3(b) and 4(b). During the restarted period, the central film thickness shows gradual reduction because of a combined actions of sudden separation occurs due to the start of entraining motion and a lack amount of lubricant to fulfill completely flooded conditions. During this period, as the speed of entraning motion increases, the wedge effect increases and the effect of squeeze is neglected as a positive value occurs; see Figure 3(d) to 3(f) and 4(d) to 4(h).
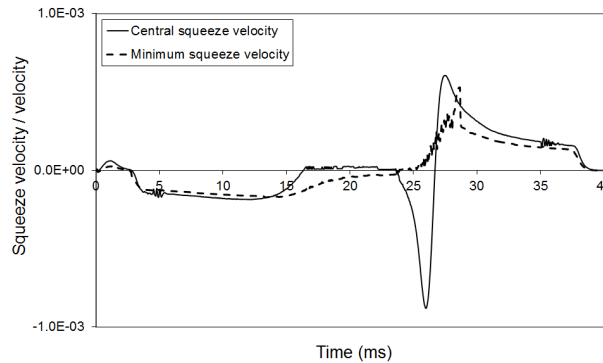
Figure 6. Squeeze ratio against time for smooth conjunction.

The following part of this study is interested in studying the characteristics of the non-smooth surfaces of the lubricated contact conjunction subjected to the variation of the entrainment velocity that is shown in Figure 2. In this case, a surface with a sine wave is proposed to study the effects of change of amplitude and wavelength of the rough contact surface on film and pressure profile at various snapshots of time. Figure 7(a) and 7(b) show the waveforms considered in the present numerical solution. Figure 7(a) shows the amplitude change, while Figure 7(b) shows the variation in wavelength.

(a) Amplitude variation

(b) Wavelength variation
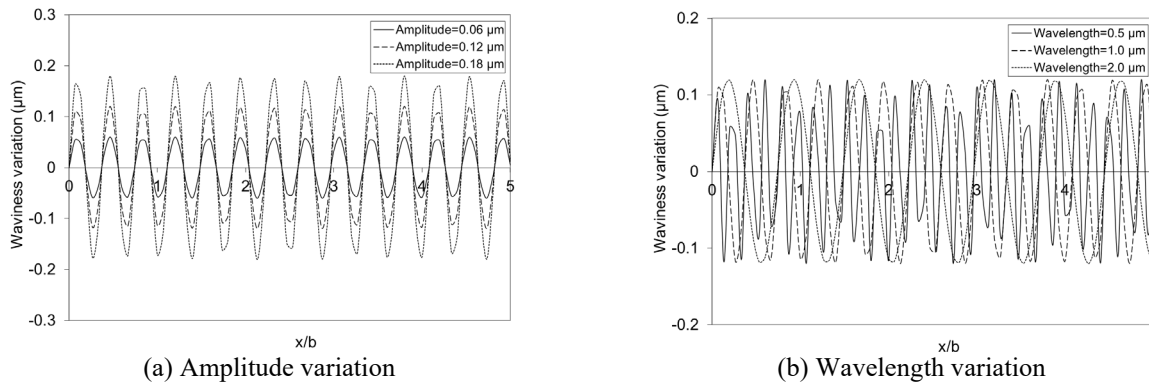
Figure 7. Waviness pattern.

Figure 8(A) and 8(B) show film profile and pressure distribution at various time steps for a deceleration/acceleration period of 14 ms and an inactive period of 7 ms under different surface amplitude waviness values ranging from 0.06 μm to 0.18 μm at wavelength value of 1.0 μm. In the same figures, film thickness and pressure profiles are presented with a smooth contact surface for the same working parameters for the purpose of comparison. It is clear that, in general, contact of a wavy surface leads to random variations of film and pressure profiles at various time steps. As the waviness amplitude values increase from 0.06 μm to 0.18 μm, large fluctuations in film and pressure profiles occur. The greater fluctuations in the pressure profiles as the waviness amplitude increases are attributed to the greater resistance of the liquid flow to contact due to the presence of the ripple. Therefore, to satisfy the flow continuity, a higher local pressure will be generated. Similar behaviour was also shown by Punit and Niraj [19] and Huang and Wang [30]. It can also be shown that the film and pressure profile shape for the wavy surface case are almost the same as previously described for the smooth surface case at various time steps; the only difference is that the waviness is imposed on the film and pressure profiles.

(A) Film thickness profile

(a)

(b)

(c)

(d)

(e)

(f)

(g)

(h)

(B) Pressure distribution

(a)

(b)
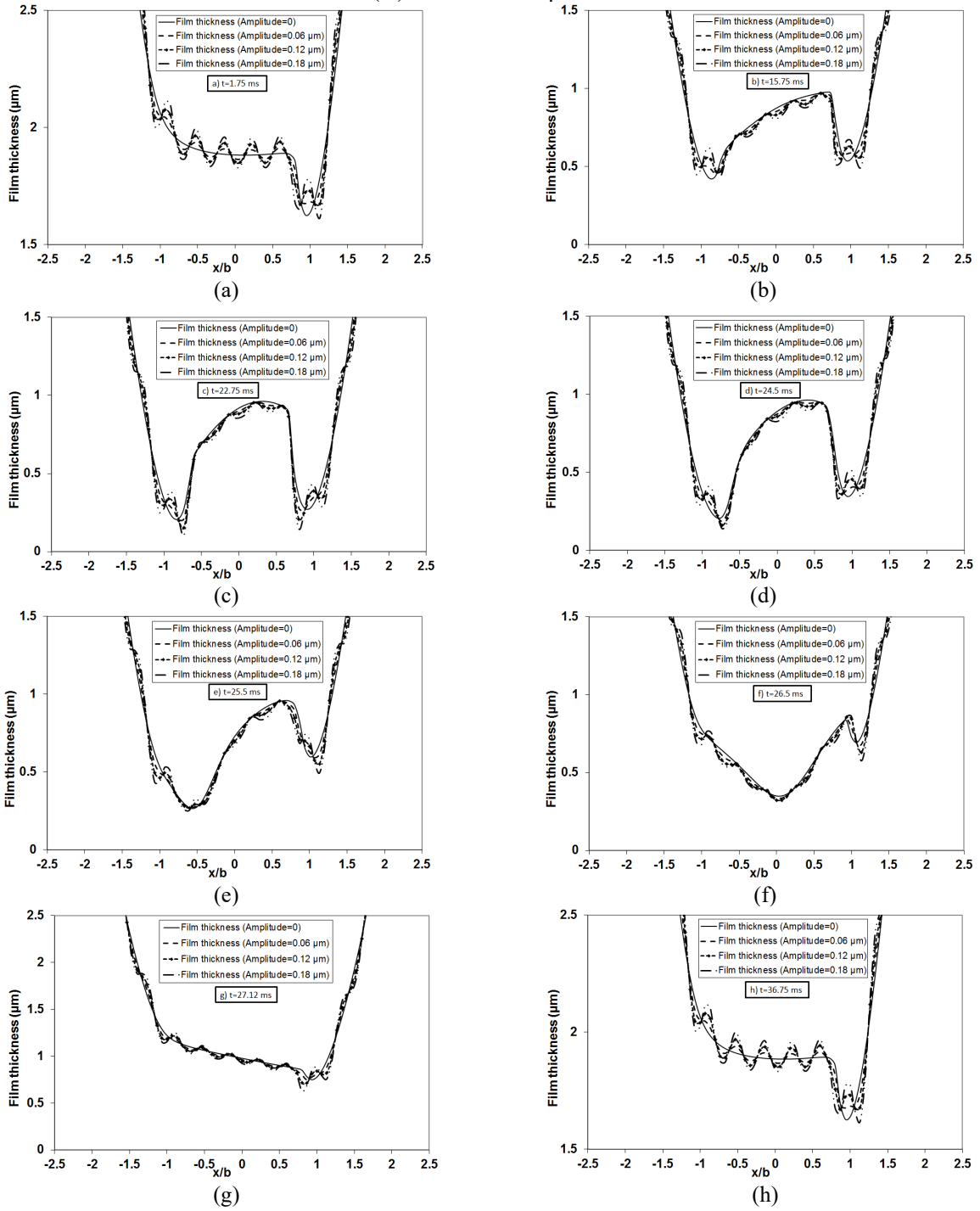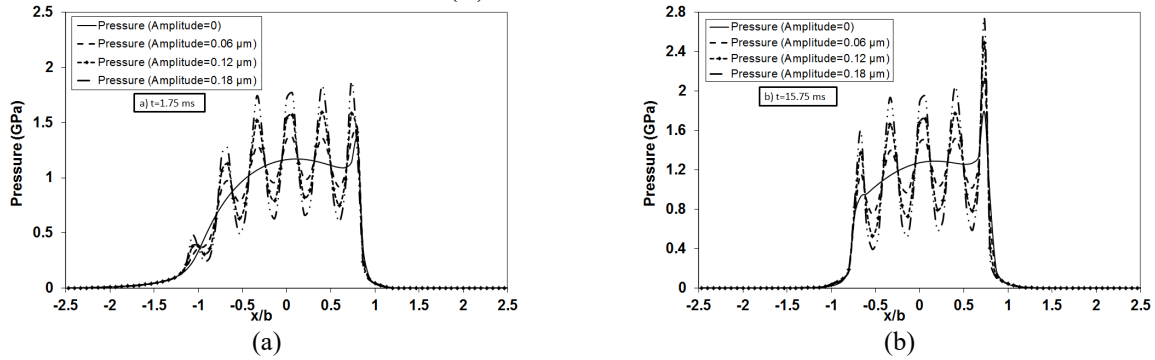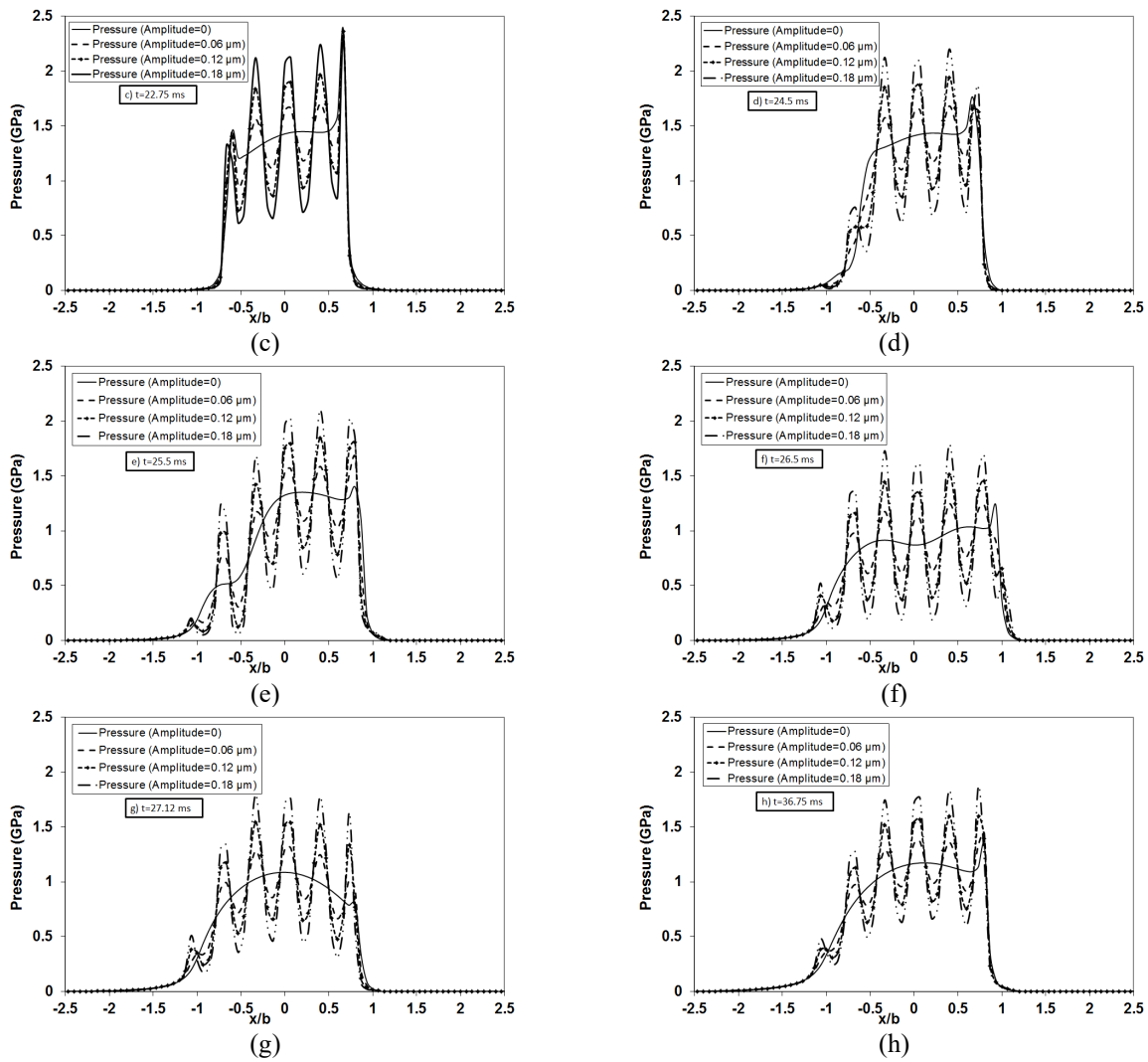
Figure 8. Numerical prediction of (A) film profile and (B) pressure distribution in the contact center under different amplitude waviness with a wavelength of 1.0 μm.

Figure 9 shows the characteristics of the lubricated wavy conjunction presented by central and maximum pressure and central and minimum film thickness with time for different amplitudes of waviness ranging from 0.06 μm to 0.18 μm at wavelength waviness of 1.0 μm for a deceleration/acceleration period of 14 ms and an inactive period of 7 ms. It is clear that the same behaviour for the central and maximum pressure and the central and minimum film thickness as that for the smooth surface contact described above and shown in Figure 5. The central and maximum pressures increase as the amplitude value increases, and the central and minimum film thickness decrease as the amplitude value increases. At the uniform entraining speed of 0.5 m/s, the values of the central pressure are 1.15 GPa, 1.34 GPa, 1.53 GPa and 1.71 GPa and the values of maximum pressure are 1.6 GPa, 1.7 GPa, 2.14 GPa and 2.25 GPa for smooth surface, 0.06 μm, 0.12 μm, 0.18 μm amplitude waviness variation, respectively. The central film thickness is 1.84 μm, 1.83 μm, 1.82 μm and 1.81 μm and the minimum film thickness is 1.35 μm, 1.3 μm, 1.25 μm and 1.2 μm for smooth surface, 0.06 μm, 0.12 μm, 0.18 μm amplitude waviness variation, respectively. It can be observed that an increase in the amplitude of the roughness results in a tendency of the minimum film thickness towards a zero value and the final result being the failure of the two contact surfaces.

Film thickness profile and pressure distribution comparisons under various surface wavelengths of 0.5 μm to 2.0 μm at various time steps during speed variation shown in Figure 2 for the same working conditions mentioned previously are shown in Figure 10(A) and 10(B) at an amplitude waviness of 0.12 μm for a deceleration/acceleration period of 14 ms and an inactive period of 7 ms. It is shown that the variation in film thickness and pressure amplitude becomes more noticeable when the surface wavelength is reduced from 2.0 μm to 0.5 μm. The minimum film thickness decreases as the surface wavelength decreases. In fact, this is due to greater flow resistance at sharp asperities, see Punit and Niraj [19] and Huang and Wang [30].
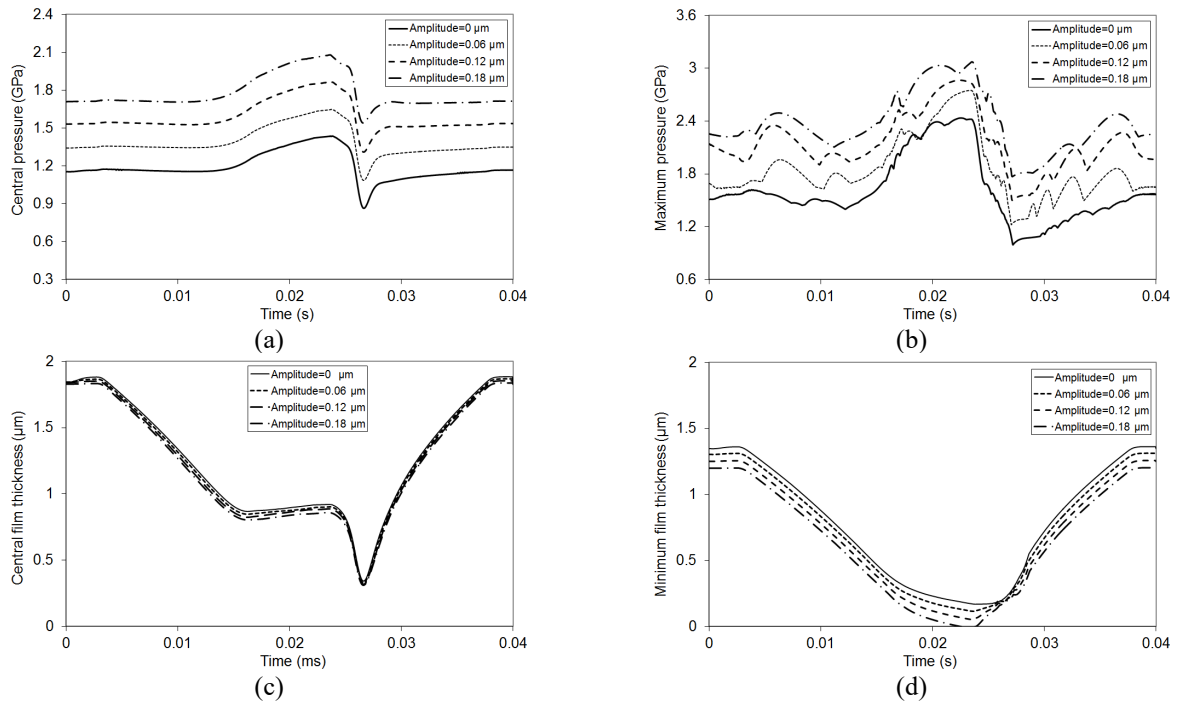
Figure 9. Characteristic of the lubricated conjunction under different amplitude waviness for a wavelength of 1.0 μm.

(A) Film thickness profile

(B) Pressure distribution
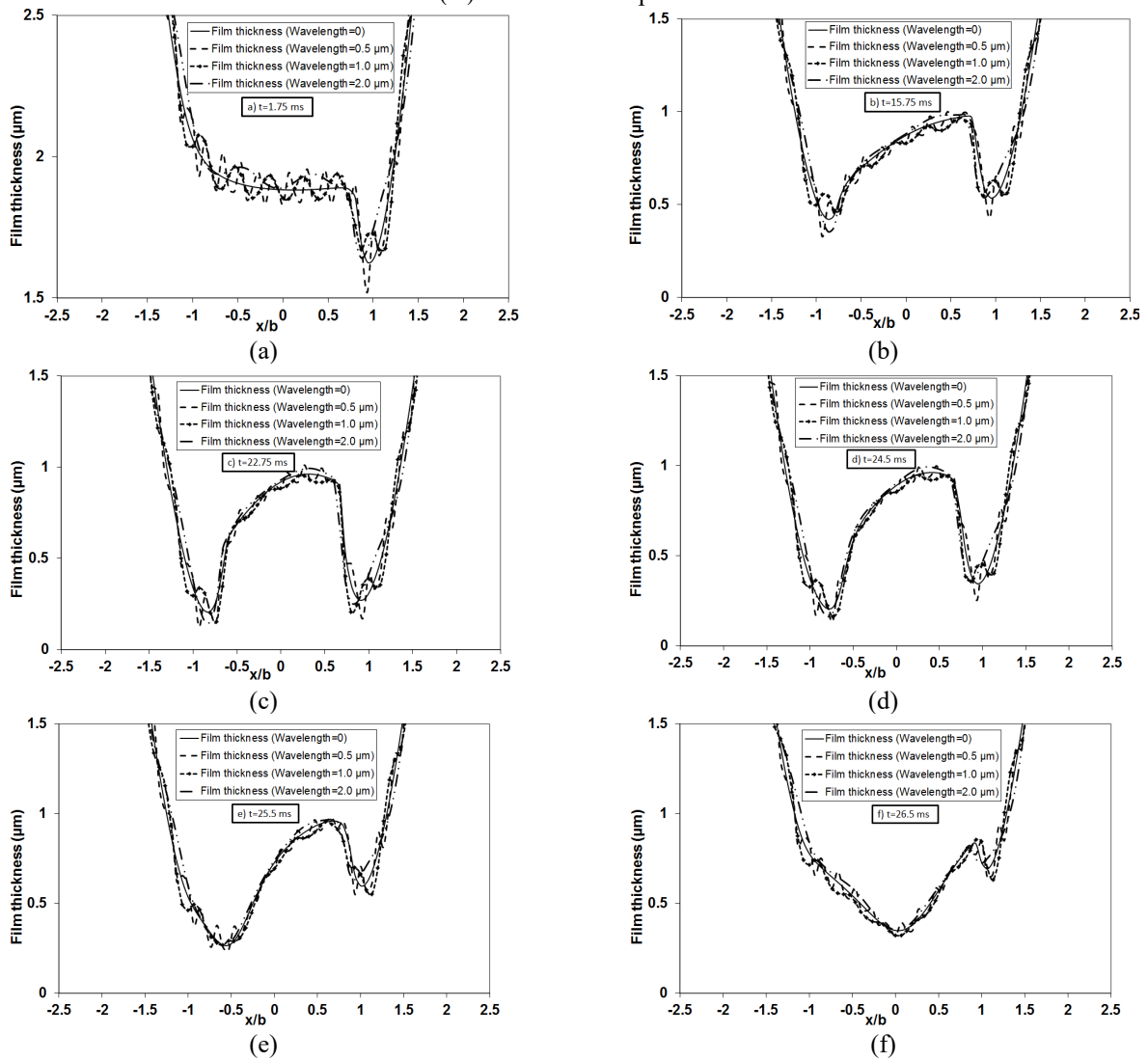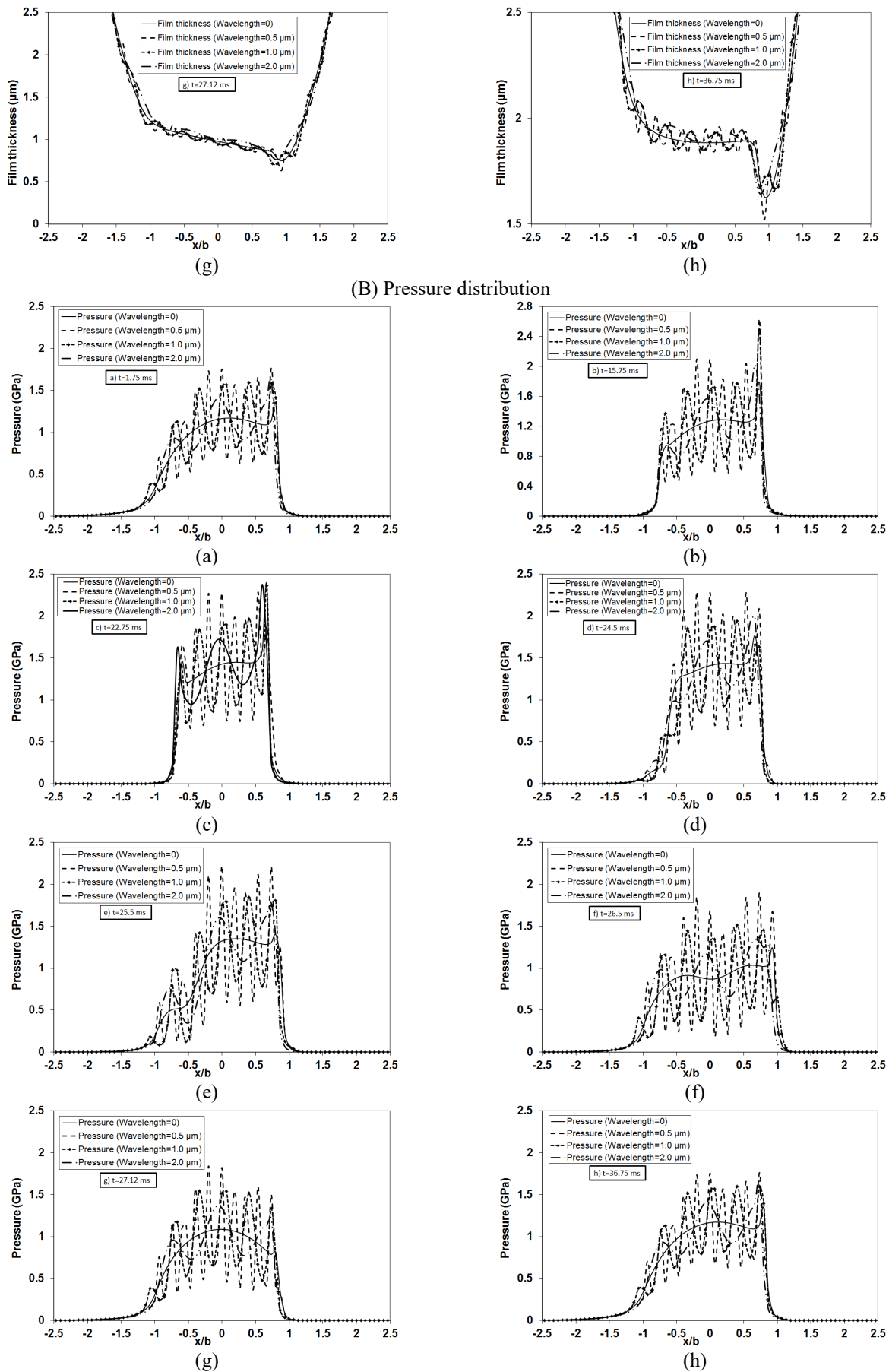
Figure 10. Numerical prediction of (A) film profile and (B) pressure distribution in the contact center under different wavelengths for amplitude waviness of 0.12 µm.

Figure 11 shows the characteristics of the lubricated conjunction presented by central and maximum pressure and central and minimum film thickness with time for various wavelength waviness ranging from 0.5 µm to 2.0 µm at an

amplitude waviness of 0.12 µm for a deceleration/acceleration period of 14 ms and an inactive period of 7 ms. It is seen that the same behaviour for the film thickness and pressure as that for the smooth contact surface described before and presented in Figure 5. As the wavelength value increases, the center pressure and maximum pressure of the contacts decrease, while at the same time increasing the center and minimum film thickness. Initially, at the uniform entraining speed of 0.5 m/s, the central pressure values are 1.15 GPa, 1.75 GPa, 1.53 GPa, and 1.38 GPa, and the maximum pressure values are 1.6 GPa, 2.3 GPa, 2.14 GPa, and 2.0. GPa for smooth surface, 0.5 µm, 1.0 µm, and 2.0 µm wavelength variation, respectively. The central film thickness is 1.84 µm, 1.83 µm, 1.82 µm and 1.80 µm and the minimum film thickness is 1.35 µm, 1.33 µm, 1.27 µm, and 1.23 µm for smooth surface, 0.5 µm, 1.0 µm, and 2.0 µm wavelength waviness variation, respectively.
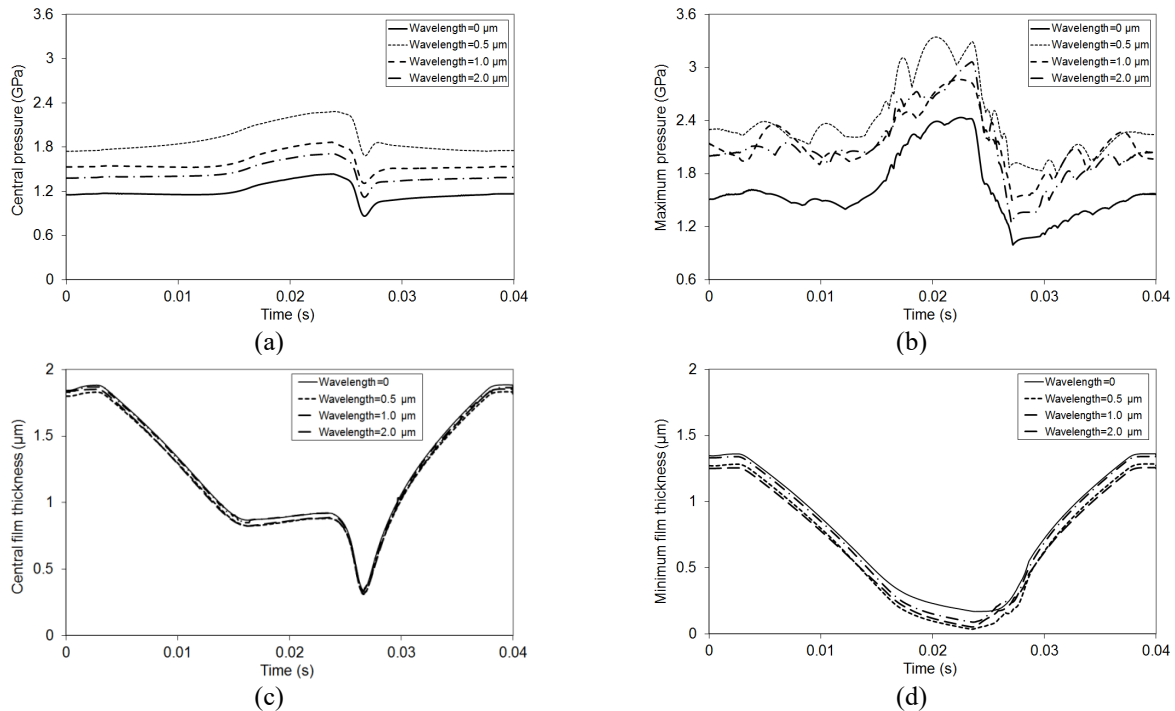
Figure 11. Characteristics of the lubricated conjunction under different wavelength waviness for amplitude of 0.12 µm.

The effect of increasing the stop period on the characteristics of the lubricated conjunction for smooth and wavy contact surfaces is presented in Figure 12. In this case, the total period time is 0.1 sec and the inactive period is 0.05 sec for the same deceleration/acceleration period of 0.014 sec and for the same operation condition of a maximum speed of 0.5 m/s and an applied contact load of 75 N for a wavy surface of 0.06 µm amplitude and a wavelength of 1.0 µm. Initially, at a maximum entrainment speed of 0.5 m/s, the central pressure, maximum pressure, central film thickness, and minimum film thickness values for the smooth surface case are 1.1 GPa, 1.5 GPa, 1.85 µm, and 1.35 µm respectively, while those obtained for the case of a wavy surface are 1.17 GPa, 1.73 GPa, 1.88 µm, and 1.3 µm, respectively. It is clear that, during this period, the central and maximum pressure values increase for the wavy surface and the center and minimum film thicknesses values decrease compared to the smooth contact surface. During the inactive period, the film thickness at the center of the contact is uniform at a value of 1.1 µm, followed by construction before it increases to its steady-state value of 1.85 µm as the entraining speed reaches a maximum value of 0.5 m/s. During this period, the minimum film thickness is reduced and reaches zero in the case of rough contact surfaces by increasing stop time. Therefore, for a long drop period, the mating surfaces stick together, and the oil film cannot separate the two mating surfaces. Both the central and maximum pressures have approximately the same characteristics. The central pressure during the inactive period is uniform at approximately a value of 1.42 GPa and 1.71 GPa for smooth and wavy surfaces, respectively, followed by a drop in the central pressure before it increases to its steady-state value of 1.1 GPa and 1.17 GPa for smooth and wavy surfaces, respectively, as the entraining velocity increases to its maximum value. The maximum pressure through the inactive period increases to a uniform value of 2.25 GPa and 2.55 GPa for smooth and wavy surfaces, respectively, followed by a drop in the maximum pressure before it increases to its steady-state value of 1.5 GPa and 1.73 GPa for smooth and wavy surface respectively, as the entraining velocity increases to its maximum value.
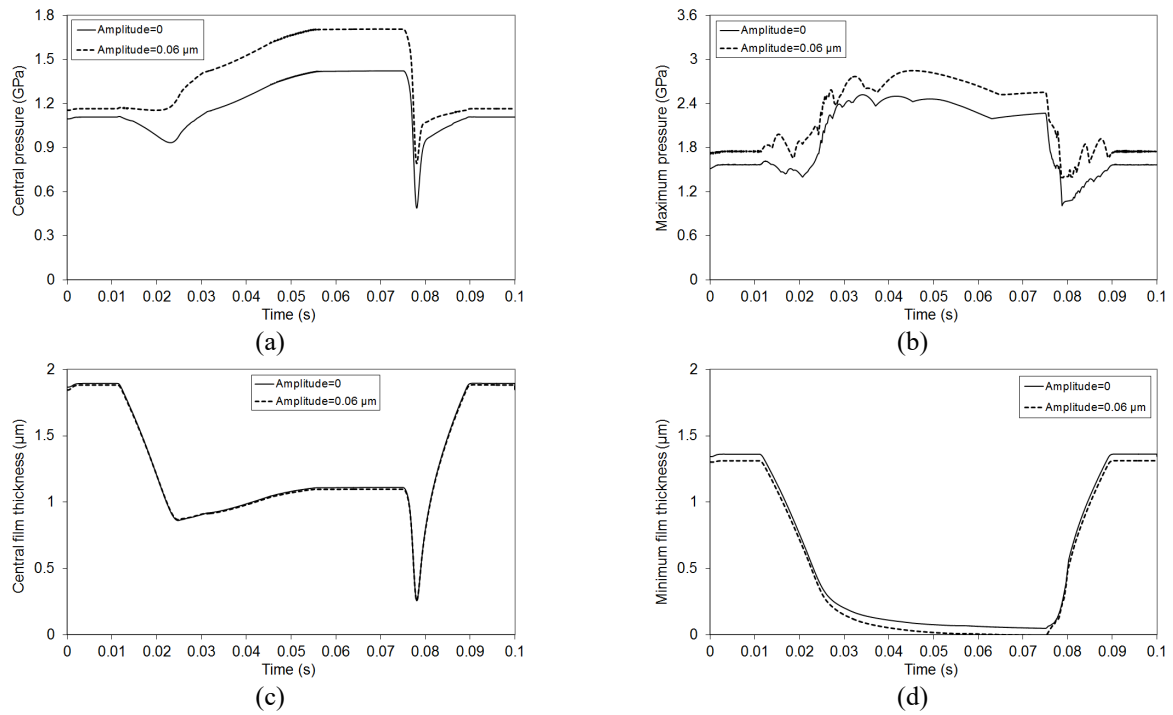
Figure 12. Characteristics of the lubricated conjunction for inactive period of 0.05 sec.

Finally, the effect of varying deceleration/acceleration intervals on a non-steady oil film and pressure build-up for a contact of smooth and rough surfaces is discussed and analyzed in this section for an applied contact load of 75 N and a maximum entrainment speed of 0.1 m/s. In this case, the total time interval is 2.5 sec, and the deceleration/acceleration interval varies from 0.5 sec to 0.01 sec at a fixed value of the stop time of 1.0 sec. Note that the larger the deceleration/acceleration periods, the smaller the deceleration/acceleration and vice versa. Figure 13 shows the effect of varying deceleration/acceleration periods on a non-steady oil film and pressure build-up for smooth contact surfaces. Initially, at the uniform entraining velocity, the central, maximum pressure and the central, minimum film thickness values are 1.1 GPa, 1.1 GPa, 0.72 μm, 0.42 μm, respectively. At the end of the deceleration phase, it is seen that reducing the deceleration/acceleration period (increasing acceleration/deceleration) leads to an increase in the central and minimum film thicknesses. This means that the central and minimum film thickness at the end of the deceleration/acceleration period is smaller for the deceleration/acceleration period of 0.5 sec than those for the deceleration periods of 0.1 sec, 0.05 sec, and 0.01 sec. This feature is attributed as the deceleration/acceleration periods decrease; the oil film does not have time to come out of the contact surface, so the center and minimum film thickness increase. This phenomenon can also be explained by referring to Figure 14, where the squeeze ratio versus time is presented for various deceleration/acceleration periods of 0.5 sec, 0.1 sec, 0.05 sec, and 0.01 sec at a fixed inactive period of 1.0 sec. It can be observed that, as the deceleration/acceleration periods decrease, the squeeze ratio of the largest negative value occurs, resulting in an increase in the central and minimum film thickness. Furthermore, it is clear that the central and maximum pressure increase during the stop time interval with the decrease of the deceleration/acceleration period.

Figure 15 shows the effect of deceleration/acceleration period variation on a transient oil film and pressure build-up for a wavy surface with a 0.03 μm amplitude and a wavelength of 1.0 μm for the same condition mentioned previously. Initially, at the maximum entrainment speed of 0.1 m/s, the central, maximum pressure and the central, minimum film thickness values are 1.15 GPa, 1.23 GPa, 0.71 μm and 0.41 μm, respectively. At the end of the deceleration phase, it is obvious that the decrease in the deceleration/acceleration periods results in an increase in the central film thickness and does not affect the minimum film thickness. This means that the minimum film thickness tends to zero at the end of the deceleration period regardless of the deceleration/acceleration periods. Comparing Figure 13 and 15, it is clear that the central and minimum film thickness at the end of the deceleration period are smaller for the case of the wavy surface shown in Figure 15 than those shown in Figure 13 for the smooth surface for different decelerations/acceleration periods. This feature is due to the fact that surface roughness reduces fluid flow by reducing the area available for flow, leading to a reduction in the central and minimum film thicknesses.
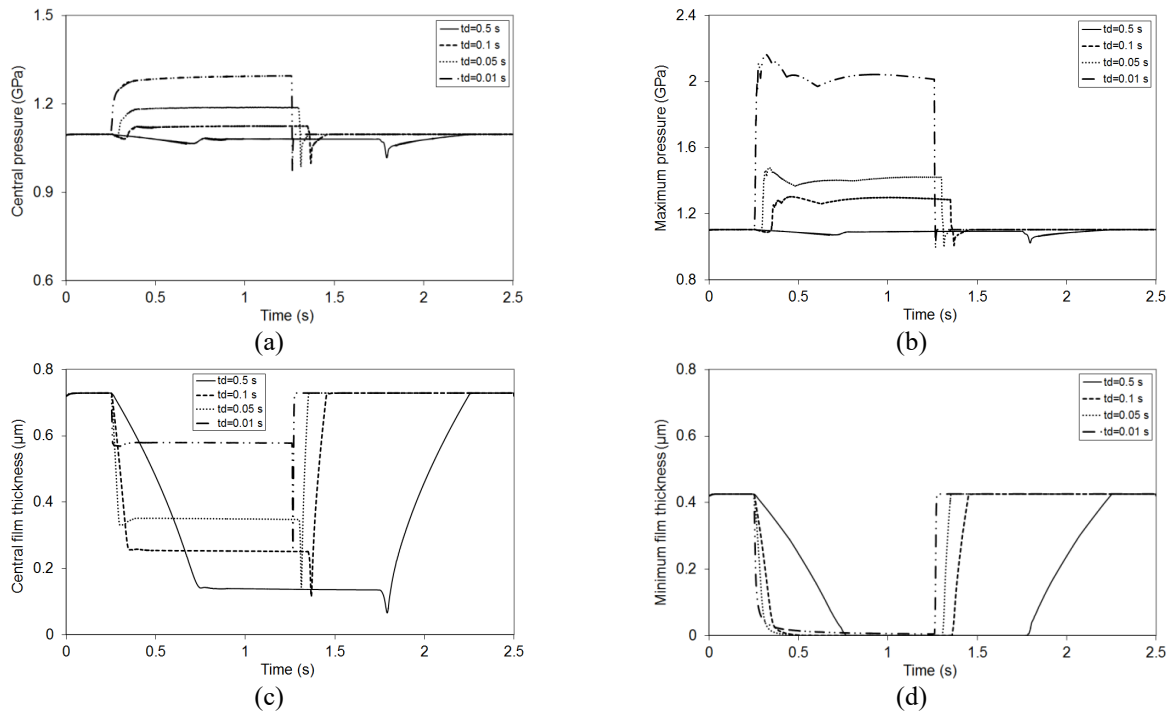
Figure 13. Characteristics of the lubricated smooth conjunction for different deceleration/acceleration periods of time stop 1.0 sec.
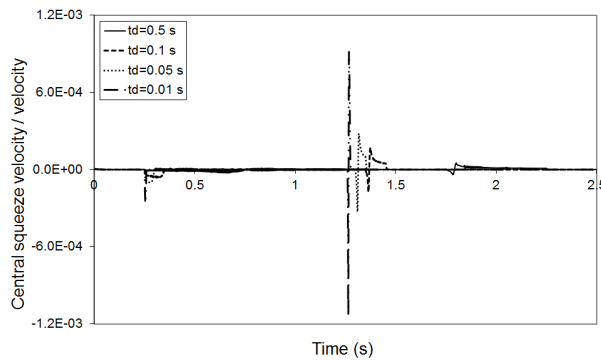
Figure 14. Central squeeze ratio versus time for smooth conjunction for various deceleration/acceleration periods.

Figure 16 shows the squeeze ratio versus time for different deceleration/acceleration periods for a wavy surface. It is clear that the squeeze of maximum negative value occurs at the lowest of the deceleration/acceleration period. The characteristics are similar for the central and maximum pressure shown in Figure 15 for wavy surfaces and those shown in Figure 13 for smooth surfaces, except that the central and maximum pressure values increase for the wavy surface due to the amplitude of the roughness, which causes greater resistance to the flow and thus more pronounced pressure; see Punit and Niraj [19] and Huaiju Liu [31]. Unfortunately, no other previous numerical or experimental study of elastohydrodynamic lubrication contact problem exists where the contact of undulating surfaces undergoes intermittent velocity changes for comparison. This area requires further research effort, as surface contact in real-world applications can experience changes in speed, shape, and load simultaneously, and it is hoped that this and other studies will lead to further research.

(c)   (d)
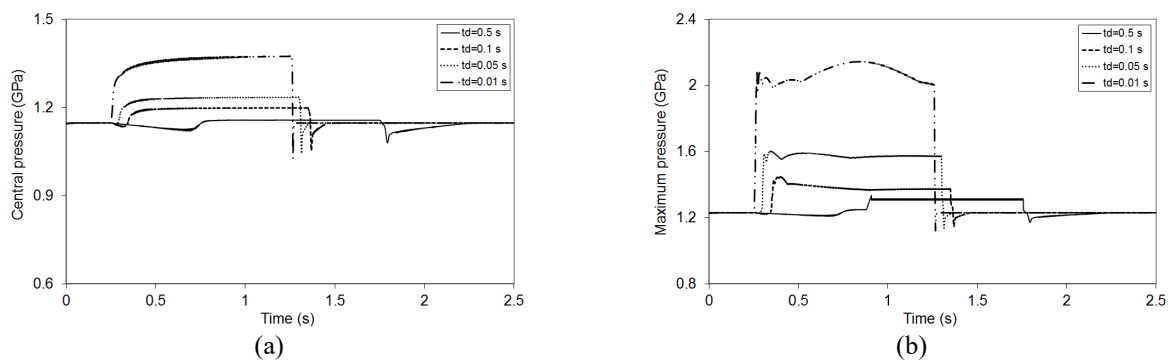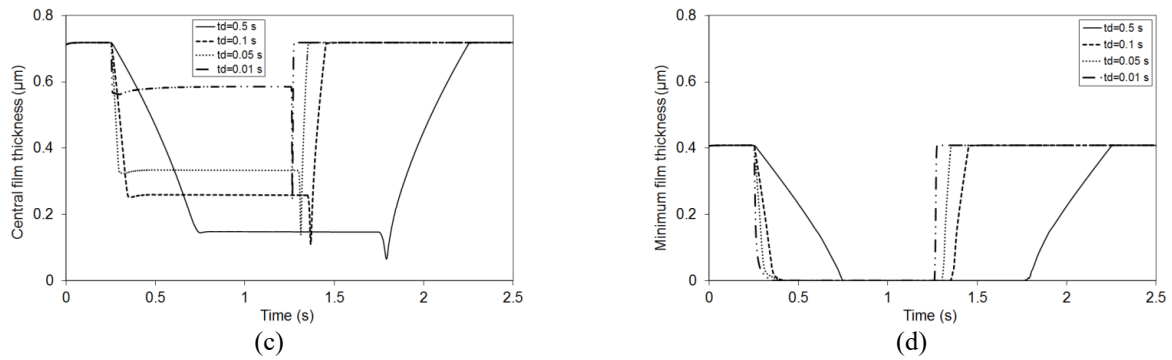
Figure 15. Characteristics of the lubricated wavy conjunction for different deceleration/acceleration periods of time stop 1.0 sec.
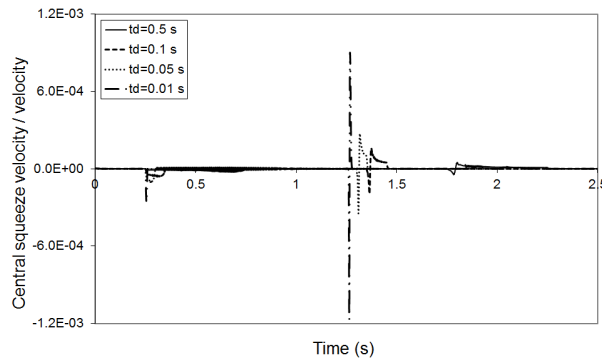
Figure 16. Central squeeze ratio versus time for wavy conjunction for various deceleration/acceleration periods.

CONCLUSION

In this paper, characteristics of transient elastohydrodynamic lubrication of both smooth and wavy surface contacts exposed to intermittent motion are discussed. Non-steady Reynolds' equation with a film thickness equation incorporating surface contact of sinusoidal waves is presented to investigate the effect of amplitude and wavelength changes on the film thickness profile and pressure distribution at various time steps. The effects of varying inactive periods of time and deceleration/acceleration periods on the characteristics of lubricated conjunction presented by the central and minimum film thickness and the central and maximum pressure are discussed. The results revealed that the wavy surfaces lead to fluctuations in the film profile and pressure distribution. Increasing the wave amplitude, the extra fluctuations of pressure and film profile. The change in wavelength indicates that fluctuations of film and pressure amplitude become a little more noticeable as wavelength increases. The pressure distribution and film thickness profile for the wavy contact surface case is almost the same as for the smooth contact surface case. The only difference between the two contacting surfaces is the fluctuation in pressure profile and film thickness. The central and maximum pressure increase, while the central and minimum film thickness decrease compared to the smooth contact surface. Effects of varying inactive periods on the characteristics of lubricated conjunction showed that, during a long stop period, the oil minimum film thickness reached a zero value, and as a result, the contact surfaces stick together, and the oil film fails to separate the two contacting surfaces, especially in the case of the wavy contact surface. In this case, the squeeze action is not effective in supporting the load capacity. The central and maximum pressure heights increase during the stop time interval as stop time increases. The results related to the variation of deceleration/acceleration period effects on the characteristics of lubricated conjunction revealed that a decrease in deceleration/acceleration period (increased deceleration/acceleration) results in an increase in the central and minimum film thickness at the end of the deceleration phase for a smooth contact surface and has no effect on the minimum film thickness for a rough contact surface. The minimum film thickness tends to be zero at the end of the deceleration phase regardless of the deceleration/acceleration periods for rough surfaces. The central and maximum pressure increase during the stop time interval with the decrease of the deceleration/acceleration period.

REFERENCES

[1]   R. P. Glovnea and H. A. Spikes, "Behavior of EHD films during reversal of entrainment in cyclically accelerated/ decelerated motion," *Tribol. Trans.*, vol. 45, no. 2, pp. 177-184, 2002, doi: 10.1080/10402000208982537.

[2]   R. P. Glovnea and H. A. Spikes, "The influence of lubricant upon EHD film behavior during sudden halting of motion," *Tribol. Trans.*, vol. 43, no. 4, pp. 731-739, 2000, doi: 10.1080/10402000008982402.

[3]   M. F. Al-Samieh and H. Rahnejat, "Ultra-thin lubricating films under transient conditions," *J. Phys. D: Appl. Phys.*, vol. 34, no. 7, pp. 2610-2621, 2001, doi: 10.1088/0022-3727/34/17/307.

[4]   S. Petr, K. David, K. Ivan and H. Martin, "Experimental investigation of lubrication film formation at start-up of smooth surfaces," *Science Journal*, vol. 12, no. 1, pp. 825-828, 2015, doi:10.17973/MMSJ.2015_12_201529.

[5]   C. L. Ming, Y. P. Chang and J. Sheu, "Elastohydrodynamic   lubrication of circular contacts at pure squeeze motion involving the mixture of two lubricants," *J. Mar. Sci. Technol.*, vol. 23, no. 4, pp. 516-522, 2015, doi: 10.6119/JMST-015-0325-1.

[6]   N. Ohno and S. Yamada, "Effect of high-pressure rheology of lubricants upon entrapped oil film behaviour at halting elastohydrodynami lubrication," *Proc. IMechE PartJ: J. Engineering Tribology*, vol. 221, no. 3, pp. 279-285, 2007, doi: 10.1243/13506501JET215.

[7]   P. Sperka *et al.*, "Occurrence of high pressure spike in unidirectional start–stop–start point contacts," *ASME J. Tribol.*, vol. 136, no. 4, pp. 503-510, 2014, doi: 10.1115/1.4028029.

[8]   M. F. Al-Samieh, "Theoretical investigation of transient ultra-thin lubricant film during rapid deceleration," *Tribol. Ind.*, vol. 40, no. 3, pp. 349-357, 2018, doi: 10.24874/ti.2018.40.03.02.

[9]   B. Meziane *et al.*,"Film thickness build-up in zero entrainment velocity wide point contacts," *Tribol. Int.*, vol. 144, pp. 105897, 2020, doi: 10.1016/j.triboint.2019.105897.

[10]   B. Meziane, N. Fillot and G. E. Morales-Espejel, "Synergy of viscosity wedge and squeeze under zero entrainment velocity in EHL Contacts," *Tribol. Lett.,* vol. 68, no. 3, pp. 1-16, 2020, doi: 10.1007/s11249-020-01311-y.

[11]   G. Sivayogan, R. Rahmani and H. Rahnejat, "Transient analysis of isothermal elastohydrodynamic point contacts under complex kinematics of combined rolling, spinning and normal approach," *Lubricants,* vol. 8, no. 81, pp. 1-22, 2020, doi:10.3390/lubricants8080081.

[12]   W. Duohuan, W. Jing and K. Motohiro, "Performance of EHL oil film in intermittent motion," *Tribology Online, Japanese Society of Tribologists*, vol. 13, no. 4, pp. 204-211, 2018, doi: 10.2474/trol.13.204.

[13]   D. Epstein *et al.*, "An efficient method of analyzing the effect of roughness on fatigue life in mixed-EHL contact," *Tribol. Trans.*, vol. 46, no. 2, pp. 273-281, 2003, doi: 10.1080/10402000308982626.

[14]   Q. J. Wang *et al.*, "Mixed lubrication analyses by a macro-micro approach and a full-scale mixed EHL model," *J. Tribol.*, vol. 126, no. 1, pp. 81-91, 2004, doi: 10.1115/1.1631017.

[15]   M. Masjedi and M. M. Khonsari, "On the effect of surface roughness in point-contact EHL: formulas for film thickness and asperity load," *Tribol. Int.*, vol. 82, no. 2, pp. 228-244, 2015, doi: 10.1016/j.triboint.2014.09.010.

[16]   B. Jacod, C. H. Venner and P. M. Lugt, "Influence of longitudinal roughness on friction in EHL contacts," *J. Tribol.*, vol. 126, no. 3, pp. 473-481, 2004, doi: 10.1115/1.1705664.

[17]   P. Yang, J. Cui, Z. M. Jin, and D. Dowson, "Influence of two-sided surface waviness on the EHL behavior of rolling/sliding point contacts under thermal and non-newtonian conditions," *J. Tribol.*, vol. 130, no. 4, pp. 502-514, 2008, doi: 10.1115/1.2958078.

[18]   C. Li-Ming, L. Jaw-Ren, H. Hsiang-Chen and C.Yuh-Ping, "Effects of surface roughness and flow rheology on the EHL of circular contacts with power-law fluid," *J. Mar. Sci. Technol.*, vol. 21, no. 2, pp. 175-181, 2013, doi: 10.1.1.669.244.

[19]   K. Punit and K. Niraj, "Surface roughness effects in pure sliding EHL line contacts with carreau-type shear-thinning lubricants," *World Academy of Science, Engineering and Technology International Journal of Mechanical and Mechatronics Engineering*,   vol. 8, no. 6, pp. 1112-1117, 2014, doi: 10.5281/zenodo.1093068.

[20]   L. Linlin and Y. Jiajun, "Surface roughness effects on point contact elastohydrodynamic lubrication in linear rolling guide with fractal surface topographies," *Ind. Lubr. Tribol.,* vol. 70, no. 4, pp. 589-598, 2018, doi: 10.1108/ILT-04-2017-0092.

[21]   X. Yang, Y. Li, G. Liu and J. Wang, "Effect of surface roughness on elastohydrodynamic lubrication performance of cylindrical roller bearing," *Tehnicki Vjesnik-Technical Gazette*, vol. 26, no. 3, pp. 710-721, 2019, doi: 10.17559/TV-20190104091451 .

[22]   M. F. Al-Samieh, "Surface roughness effects for newtonian and non-newtonian lubricants," *Tribol. Ind.*, vol. 41, no. 1, pp. 56-63, 2019, doi: 10.24874/ti.2019.41.01.07.

[23]   Y. Zhang, "Friction prediction for rough surfaces in an elastohydrodynamically lubricated contact," Ph.D thesis, University de Lyon, France, 2019.

[24]   J. Hansena, M. Björlinga and R. Larsson, "Mapping of the lubrication regimes in rough surface EHL contacts," *Tribol. Int.,* vol. 131, pp. 637-651, 2019, doi: 10.1016/j.triboint.2018.11.015

[25]   T. Hultqvist *et al.*, "Transient analysis of surface roughness features in thermal elastohydrodynamic contacts," *Tribology International*, vol. 144, no. 2, pp. 105915, 2020, doi: 10.1016/j.triboint.2019.105915.

[26]   T. Hultqvist, A. Vrcek, P. Marklund and R. Larsson "On waviness and two-sided surface features in thermalelastohydrodynamically lubricated line contacts," *Lubricants,* vol. 8, no. 64, pp. 1-27, 2020, doi: 10.3390/lubricants8060064.

[27]   T. Hultqvist *et al.*, "Transient plasto-elastohydrodynamic lubrication concerning surface features with application to split roller bearings," *P. I. Mech. Eng. J.-J. Eng.,* vol. 235, no. 2, pp. 453-467, 2021, doi: 10.1177/1350650120927566.

[28]   R. Gohar and H. Rahnejat, *Fundamentals of tribology*. London: Imperial College Press, 2008.

[29]   M. F.Al-Samieh, "Numerical investigation of elastohydrodynamic contacts subjected to harmonic load variation," *Ind. Lubr. Tribol.*, vol. 71, no. 6, pp. 832-841, 2019 ,doi: 10.1108/ILT-12-2018-0461.

[30]   X. Huang and Y. Wang, "Transient elastohydrodynamic lubrication analysis of spur gears running-in considering effects of solid particles and surface roughness," *Ind. Lubr. Tribol.*, vol. 68, no. 2, pp. 183-190, 2016, doi: 10.1108/ILT-05-2015-0061.

[31]   Liu. Huaiju, "Lubricated contact analysis of a spur gear pair with dynamic loads," Ph.D thesis, University of Warwick, UK, 2013.